IL NUOVO CIMENTO Vol. 31 C, N. 5-6 Settembre-Dicembre 2008
DOI 10.1393/ncc/i2008-10323-4

Numerical simulation of flow over barriers in complex terrain

T. Bodnár([2]), L. Beneš([1]) and K. Kozel([2])

([1]) *Faculty of Mechanical Engineering, Czech Technical University - Prague, Czech Republic*
([2]) *Institute of Thermomechanics, Academy of Sciences of the Czech Republic Prague, Czech Republic*

(ricevuto il 30 Ottobre 2008; approvato il 15 Dicembre 2008; pubblicato online il 27 Marzo 2009)

Summary. — This paper presents some of the results of numerical simulations of flow in the proximity of significant artificial terrain obstacles. The mathematical model is based on Reynolds averaged Navier-Stokes equations for incompressible flows. Turbulent closure of the model is obtained by a simple algebraic turbulence model. The numerical solution is carried out by the semi-implicit finite-difference scheme. The results of simple tests are presented and summarized. Model sensitivity has been studied with respect to the simulated obstacle size and shape.

PACS 92.60.Fm – Boundary layer structure and processes.

Introduction

This study has been motivated by the request to evaluate the possible effect of downwind obstacles on the deposition of wind drifted coal dust. In the presented part of this project our attention was concentrated on the detailed computation of the flow field characteristics in the vicinity of large terrain obstacles. Special attempt has been made to localize the areas where the flow is decelerating or recirculating. These flow regimes could be critical from the point of view of surface particle deposition.

The problem of flow and pollution dispersion in the vicinity of terrain obstacles was deeply explored in numerous studies in the past. Most papers deal with geometrical set-up based on low smooth hills. One of the classical experimental works is the paper [1] where the wake flows behind 2D polynomial hills are explored. Flow over 2D sinusoidal topography with different hill slopes is studied experimentally in [2] and compared with numerical simulation in [3]. The influence of multiple 2D sinusoidal hills on the flow field is investigated in experimental study [4]. Some comparisons with CFD solutions were presented there. Similar study was presented also in [5]. An experimental investigation of flow and pollution dispersion in the disturbed boundary layer flow over a ridge was

published in papers [6] and [7]. The wind tunnel study of the flow structure and pollution dispersion from point sources in the vicinity of 3D single hill was published in papers [8] and [9]. In these papers series of wind tunnel experiments is described to show the importance of three-dimensionality of the flow- (and concentration-) field. Some further material especially concerning the simulated pollution dispersion can be found in the papers [10-16].

Another large group of studies focuses on the flow over artificial obstacles rather than over smooth hills. The flow over different solid and porous fences was experimentally investigated, *e.g.*, in [17-20] or [21]. The comparison of experimental data with numerical simulations could be found in [22]. The coal dust and sand dispersion in the presence of porous fences was explored, *e.g.*, in [23-26]. The effect of tree-blocks and forest edges on the wind flow and pollution dispersion and deposition was studied, *e.g.*, in [27, 28] or [29].

Most of the above mentioned studies were focused on more or less simple geometry, usually dealing with a flat terrain with single obstacles. The case we need to solve is based on real (and thus complex) orography, where the natural terrain profile dominates the flow. The artificial obstacles placed to the flow in this case only partially modify the flow and concentration patterns. Therefore it is essential for this study to deal with the actual orography corresponding to the true domain of interest.

The complex terrain profile used in this study represents a part of the opencast coal mine where there is placed a coal storage. This storage acts as a source of coal dust which is drifted by the wind. The detailed orography profile was obtained by a combination of data from several geographical resources. In order to get maximum of realistic details a laser scan of the terrain was performed and included into the orography profile. The aim of this study is to give both qualitative and quantitative guidelines for the evaluation of the environmental impact of artificial obstacles placed downwind from the coal storage.

1. – Mathematical model

The flow in atmospheric boundary is turbulent in most simulations. The fluid motion can be thus described by the Reynolds averaged Navier-Stokes equations (RANS). The non-conservative form of the RANS system is represented by the following equations:

$$u_x + v_y + w_z = 0, \tag{1}$$

$$V_t + uV_x + vV_y + wV_z = -\frac{\nabla p}{\rho} + [KV_x]_x + [KV_y]_y + [KV_z]_z. \tag{2}$$

Here $V = col(u, v, w)$ is the velocity vector, p is pressure, ρ is density.

The turbulence model is based on the Boussinesq hypothesis on the turbulent diffusion coefficient $K = \nu + \nu_T$ which is expressed as a sum of molecular and eddy viscosity([1]). Finally the following algebraic turbulence model was used to complete the governing

([1]) The molecular viscosity is usually much smaller than the turbulent one, but it cannot be neglected because it guarantees that the turbulent diffusion coefficient K will remain stricly positive. This is important for the well posedness of the mathematical model and for the stability of the numerical solver.

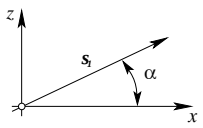

$$\frac{\partial}{\partial x} = \frac{1}{\cos\alpha}\left(\frac{\partial}{\partial s_1} - \frac{\partial}{\partial z}\sin\alpha\right)$$

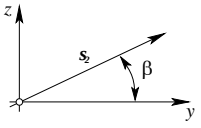

$$\frac{\partial}{\partial y} = \frac{1}{\cos\beta}\left(\frac{\partial}{\partial s_2} - \frac{\partial}{\partial z}\sin\beta\right)$$

$$\overleftarrow{\delta_s} = \frac{\mathsf{V}_i - \mathsf{V}_{i-1}}{\Delta s^-}$$

$$\overrightarrow{\delta_s} = \frac{\mathsf{V}_{i+1} - \mathsf{V}_i}{\Delta s^+}$$

$$\delta_s = \frac{1}{2}(\overleftarrow{\delta_s} + \overrightarrow{\delta_s})$$

Fig. 1. – Local coordinate transformation.

system:

$$K = \nu + \nu_T, \qquad \text{where} \qquad \nu_T = \ell^2 \left[\left(\frac{\partial u}{\partial z}\right)^2 + \left(\frac{\partial v}{\partial z}\right)^2\right]^{1/2}. \tag{3}$$

The mixing length ℓ is computed according to the following formula:

$$\ell = \frac{\varkappa(z+z_0)}{1+\varkappa\frac{(z+z_0)}{\ell_\infty}}, \qquad \text{where} \qquad \ell_\infty = \frac{27\,|V_G|\,10^{-5}}{f_c}. \tag{4}$$

Here $f_c = 1.1 \times 10^{-4}\,\mathrm{ms}$ denotes the Coriolis parameter and V_G is the geostrophic wind velocity at the upper boundary of domain.

2. – Numerical solution

2˙1. *Finite-difference discretization.* – To discretize the governing system the non-orthogonal, structured, boundary (*i.e.* terrain), following mesh was constructed. Because of the mesh non-orthogonality it was necessary to transform the equations from the x-y-z coordinates to the mesh-wise directional local coordinate system s_1-s_2-z (see fig. 1).

To simplify the notation of discretized equations the operators of differences are introduced. The symbol δ_s denotes the central difference with respect to the direction $\boldsymbol{s}$. Similarly the $\overrightarrow{\delta_s}$, $\overleftarrow{\delta_s}$ denote the forward and backward differences.

2˙2. *Semi-implicit finite-difference scheme.* – The system of governing equations (5), (6) should be transformed into the above-described mesh-wise local coordinate system.

$$u_x + v_y + w_z = 0, \tag{5}$$

$$V_t + uV_x + vV_y + wV_z = \underbrace{-\frac{\nabla p}{\rho} + [KV_x]_x + [KV_y]_y + [KV_z]_z}_{=\mathrm{RHS}}. \tag{6}$$

Using the local coordinate transformation, this system could be rewritten so that the continuity equation (5) takes the form

$$\frac{u_{s_1}}{\cos\alpha} + \frac{v_{s_2}}{\cos\beta} + w_z - u_z\tan\alpha - v_z\tan\beta = 0. \tag{7}$$

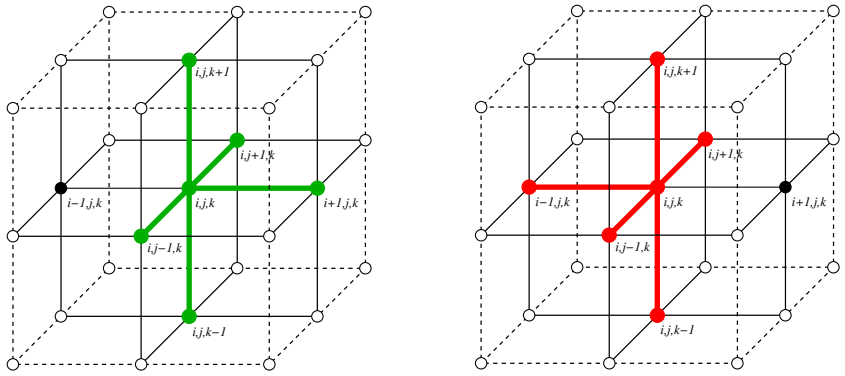

Time-level n Time-level $n+1$

Fig. 2. – Computational stencil for semi-implicit FD scheme.

The momentum equations will then be modified to the following form([2]):

$$V_t + \tilde{u}V_{s_1} + \tilde{v}V_{s_2} + \tilde{w}V_z = \widetilde{RHS}. \tag{8}$$

The modified coefficients are defined as follows:

$$\tilde{u} = \frac{u}{\cos\alpha}\,, \qquad \tilde{v} = \frac{v}{\cos\beta}\,, \qquad \tilde{w} = w - u\tan\alpha - v\tan\beta.$$

The right-hand side is transformed in a similar way. The left-hand side of momentum equations is discretized by the following way:

$$\begin{aligned}
V_t &\sim \overrightarrow{\delta_t}\mathsf{V}^n_{i,j,k},\\
\tilde{u}V_{s_1} &\sim \frac{1}{2}\left(\tilde{u}^n_{i+1/2}\overrightarrow{\delta_{s_1}}\mathsf{V}^n_{i,j,k} + \tilde{u}^n_{i-1/2}\overleftarrow{\delta_{s_1}}\mathsf{V}^{n+1}_{i,j,k}\right),\\
\tilde{v}V_{s_2} &\sim \frac{1}{2}\left\{\frac{1}{2}\left(\tilde{v}^n_{j+1/2}\overrightarrow{\delta_{s_2}}\mathsf{V}_{i,j,k} + \tilde{v}^n_{j-1/2}\overleftarrow{\delta_{s_2}}\mathsf{V}_{i,j,k}\right)^n\right.\\
&\quad\left.+\frac{1}{2}\left(\tilde{v}^n_{j+1/2}\overrightarrow{\delta_{s_2}}\mathsf{V}_{i,j,k} + \tilde{v}^n_{j-1/2}\overleftarrow{\delta_{s_2}}\mathsf{V}_{i,j,k}\right)^{n+1}\right\},\\
\tilde{w}V_z &\sim \frac{1}{2}\left\{\frac{1}{2}\left(\tilde{w}^n_{k+1/2}\overrightarrow{\delta_z}\mathsf{V}_{i,j,k} + \tilde{w}^n_{k-1/2}\overleftarrow{\delta_z}\mathsf{V}_{i,j,k}\right)^n\right.\\
&\quad\left.+\frac{1}{2}\left(\tilde{w}^n_{k+1/2}\overrightarrow{\delta_z}\mathsf{V}_{i,j,k} + \tilde{w}^n_{k-1/2}\overleftarrow{\delta_z}\mathsf{V}_{i,j,k}\right)^{n+1}\right\}.
\end{aligned}$$

The coefficients $\tilde{u}$, $\tilde{v}$, $\tilde{w}$ are fixed at the time-level n in order to linearize locally the system to obtain an Oseen-like iterative solver. The combination of different asymmetric space

([2]) The $\widetilde{RHS}$ and $\overline{RHS}$ are the modified right-hand sides.

discretization at time levels n and $n+1$ allows us to construct finally the numerical scheme that is centered and second order in both space and time. The computational stencil is different for discretization at time level n and $n+1$ (see fig. 2). The dissipative terms on the right-hand side are approximated in the same manner. Using this discretization, the system of linear algebraic equations in each column of grid-points is obtained:

$$a_1 \mathsf{V}^{n+1}_{i,j+1,k} + a_2 \mathsf{V}^{n+1}_{i,j,k} + a_3 \mathsf{V}^{n+1}_{i,j-1,k} + a_4 \mathsf{V}^{n+1}_{i,j,k+1} + a_5 \mathsf{V}^{n+1}_{i,j,k-1} = \overline{RHS}. \tag{9}$$

This system is solved iteratively in vertical plane $i = \text{const}$. So the five-diagonal system is converted into the three-diagonal one.

$$a_5 \mathsf{V}^{\eta+1}_{i,j,k-1} + a_2 \mathsf{V}^{\eta+1}_{i,j,k} + a_4 \mathsf{V}^{\eta+1}_{i,j,k+1} = \overline{RHS} - a_1 \mathsf{V}^{\eta}_{i,j+1,k} - a_3 \mathsf{V}^{\eta+1}_{i,j-1,k}. \tag{10}$$

The η denotes here the iterative index. Usually after 3–5 iterations the values of $\mathsf{V} = (u, v, w)^T$ are known with sufficient accuracy. Exactly the same solution scheme can also be used for the scalar transport equations.

In the steady (or quasi-steady) problems the artificial compressibility method can be used and in such a case the pressure is updated from the modified continuity equation.

$$p_t = -(u_x + v_y + w_z). \tag{11}$$

Also here the above-described semi-implicit discretization is used to keep the consistency with the momentum equations solver.

In order to improve the convergency of this method for high Reynolds numbers, the artificial viscosity terms $\mathsf{DV}^n_{i,j,k}$ are added. Then the solution algorithm skips to the time level $(n+1)$.

2˙3. *Artificial viscosity.* – The combination of artificial dissipation of second and fourth order is used.

$$\begin{aligned}
\mathsf{DV}^n_i &= \mathsf{D}^2\mathsf{V}^n_i + \mathsf{D}^4\mathsf{V}^n_i, \\
\mathsf{D}^2\mathsf{V}^n_i &= \tilde{\epsilon}_2 \Delta x^3 \frac{\partial}{\partial x} |\mathsf{V}_x| \mathsf{V}_x = \tilde{\epsilon}_2 \Delta x^2 (\epsilon_{i+1/2} \mathsf{V}_x - \epsilon_{i-1/2} \mathsf{V}_x), \\
\epsilon_{i+1/2} &= \begin{cases} |\mathsf{V}_{i+1} - \mathsf{V}_i| & \text{for } |\mathsf{V}_{i+1} - \mathsf{V}_i| < \frac{K}{10}, \\ \frac{K}{10} & \text{for } |\mathsf{V}_{i+1} - \mathsf{V}_k| \geq \frac{K}{10}, \end{cases} \\
\mathsf{D}^4\mathsf{V}^n_i &= \tilde{\epsilon}_4 \Delta x^4 \mathsf{V}_{xxxx} = \tilde{\epsilon}_4 \left(\mathsf{V}^n_{i-2} - 4\mathsf{V}^n_{i-1} + 6\mathsf{V}^n_i - 4\mathsf{V}^n_{i+1} + \mathsf{V}^n_{i+2} \right).
\end{aligned}$$

The $K = \nu + \nu_t$ is the coefficient of turbulent diffusion. The coefficients $\tilde{\epsilon}_2$, $\tilde{\epsilon}_4 \in \mathsf{R}$ are constants of order Δx^2, respectively Δx^4.

The details of the numerical discretization could be found, *e.g.*, in [30, 31, 29].

3. – Numerical results

Numerical experiments were performed in a 3D domain of the size $500 \times 250 \times 400$ meters. The bottom boundary represents a complex terrain orography. The contours of terrain elevation are shown in the following figure 3. The height difference between the

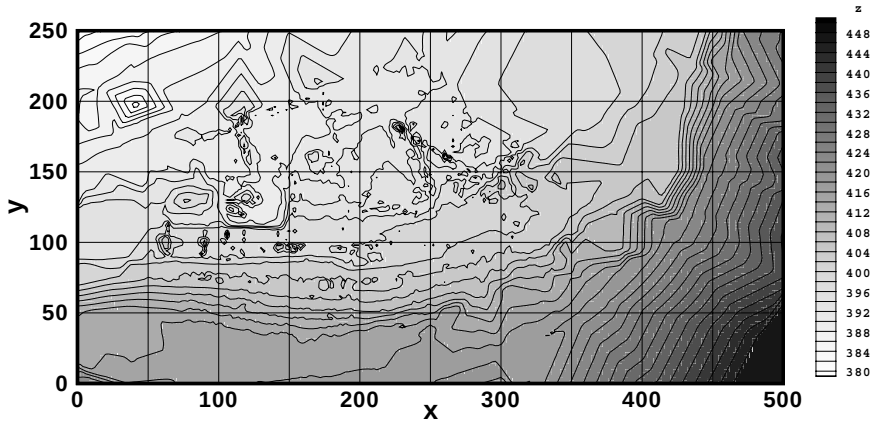

Fig. 3. – Terrain elevation contours.

highest and the lowest point of the terrain profile is about 70 meters. The wind flow in the model domain is forced by the prescribed velocity profile at the inlet ($x = 0$). The maximum velocity 10 m/s is achieved at the upper boundary of the domain.

Figure 4 shows the wind flow streamlines at near-ground level for the basic variant with no obstacles. This variant is used for reference and comparison because it represents the actual state. In order to slow down and deflect the flow we have placed different obstacles downwind from the expected source of pollution. The obstacles differ in their shape and size. The first series of experiments uses an obstacle formed by a block with horizontal size 10×60 meters which is rotated by 45 degrees with respect to mainstream flow direction. The height of the obstacles varies between 3 and 9 meters. The immersed boundary approach was used to simulate this impermeable block.

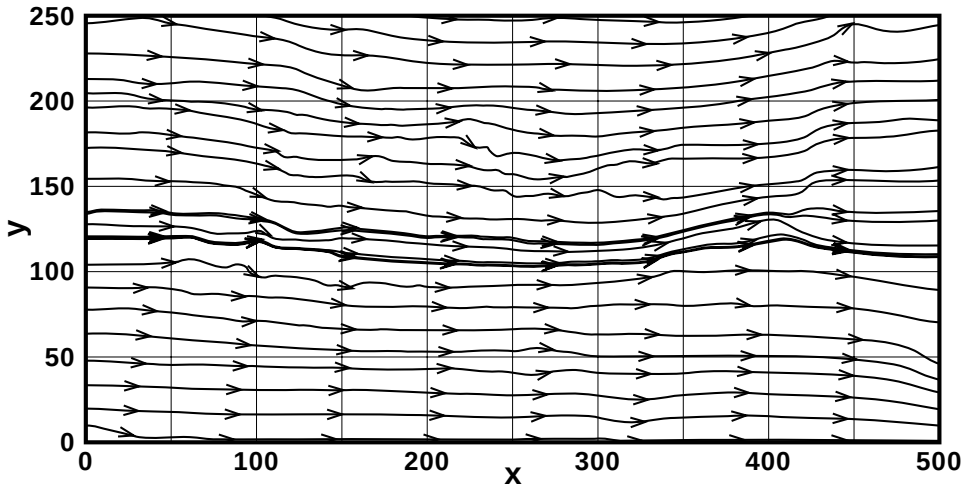

Fig. 4. – Wind flow streamlines at the near-ground level for the case without obstacles.

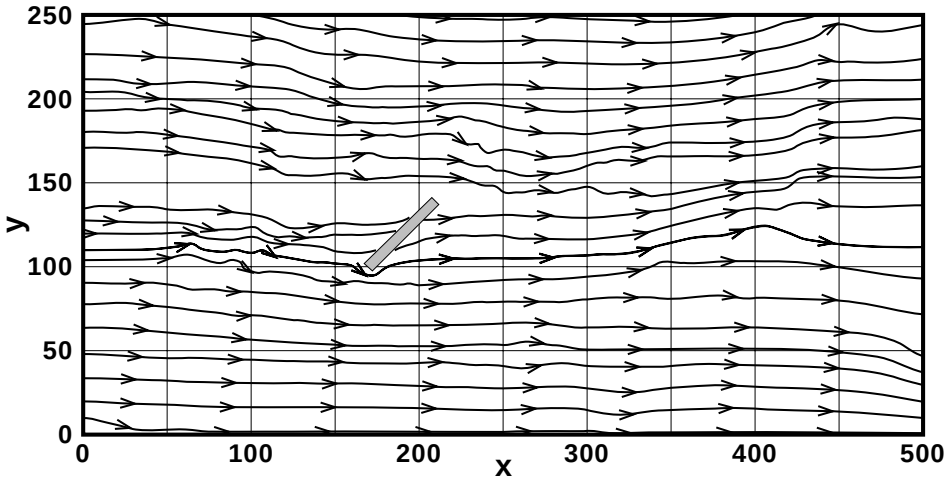

Fig. 5. – Wind flow streamlines at the near-ground level for the case with obstacle of height 3 meters.

In order to evaluate the impact of obstacle height on the flow the simulations were run for the case with single obstacle with height 3, 6 and 9 meters. The streamlines at the near-ground level for these cases are shown in figs. 5, 6 and 7. From the comparison of figs. 5, 6 and 7 it is clearly visible that the increasing height of the obstacle leads to significantly higher flow deviations. For the obstacle height 6 and 9 meters the impact of the artificial obstacle is stronger (at least locally) than the influence of the local orography. However even for the highest obstacle the flow is only disturbed locally and no larger scale flow pattern modification was observed.

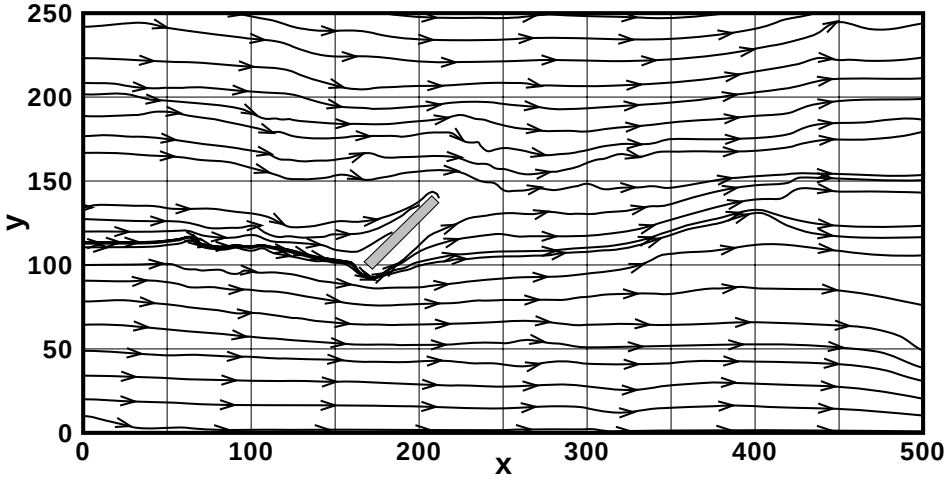

Fig. 6. – Wind flow streamlines at the near-ground level for the case with obstacle of height 6 meters.

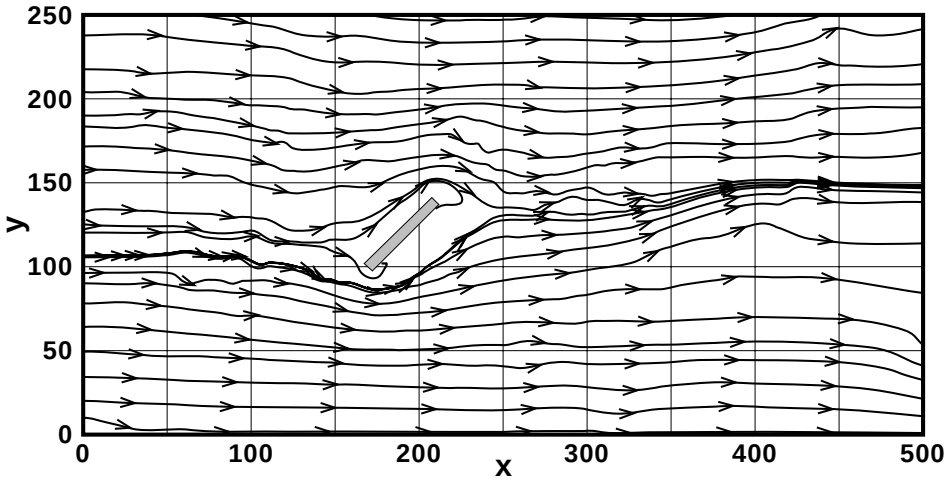

Fig. 7. – Wind flow streamlines at the near-ground level for the case with obstacle of height 9 meters.

From the technological point of view it is not possible to build at the investigated site obstacles higher than 9 meters and also the horizontal size of obstacles is strictly limited. Thus when seeking for obstacles leading to more profound flow modifications it is not possible to increase the obstacles dimensions. Therefore some other configurations of obstacles of similar size were investigated assuming that it is possible to get better results with another obstacle shape rather than larger size.

Two other variants have been tested as an attempt to increase the flow deflection while respecting the technological obstacle size limitations. Instead of one large, two

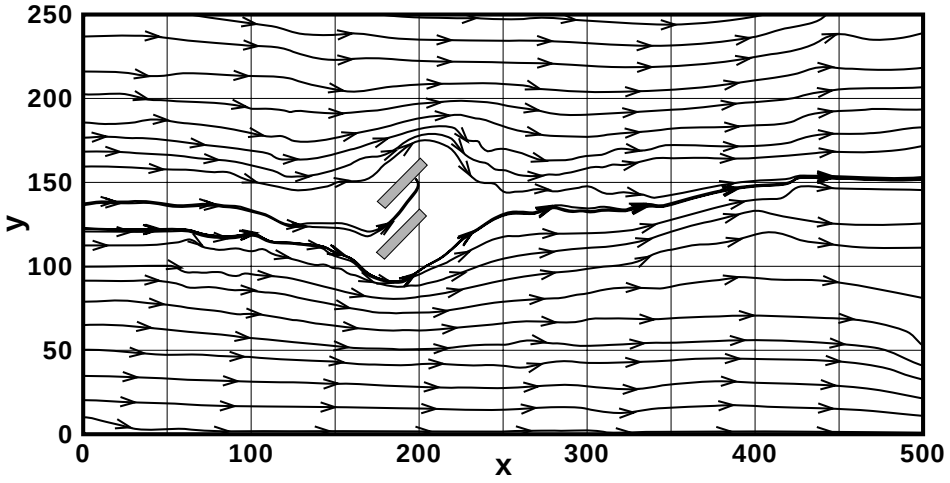

Fig. 8. – Wind flow streamlines at the near-ground level for the case with two parallel obstacles of height 9 meters.

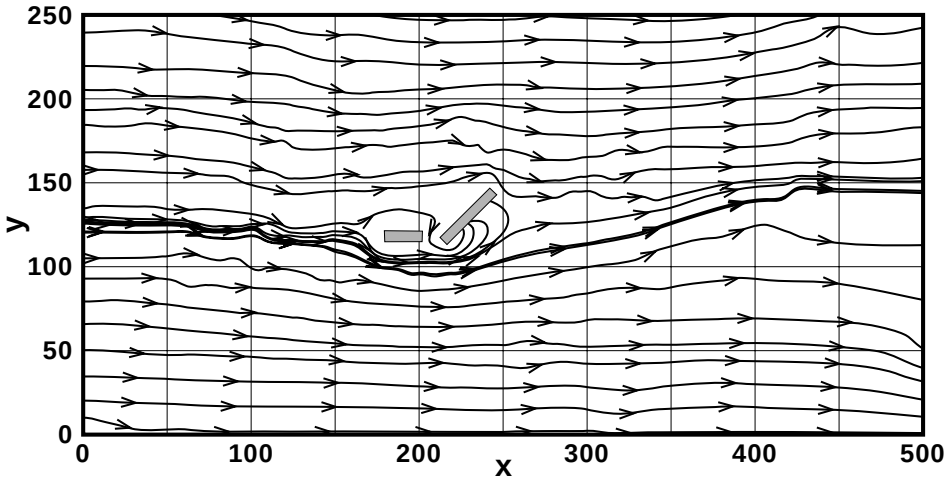

Fig. 9. – Wind flow streamlines at the near-ground level for the case with two obstacles of height 9 meters.

obstacles of smaller size and different configuration have been assumed. In both cases the height of obstacles was 9 meters. The near-ground stramlines are shown in figs. 8 and 9. The simulation results have shown that the obstacles placed in the proximity of the expected pollution source have only local impact on the flow field.

Thus it seems that it is not possible to achieve any larger scale flow deflection and modify the pollutant dispersion trajectories. The only way to influence the downstream airborne dust concentrations is to enhance the particle sedimentation. From this point of view it is evident that the slower the flow is, the more particles will fall out of the

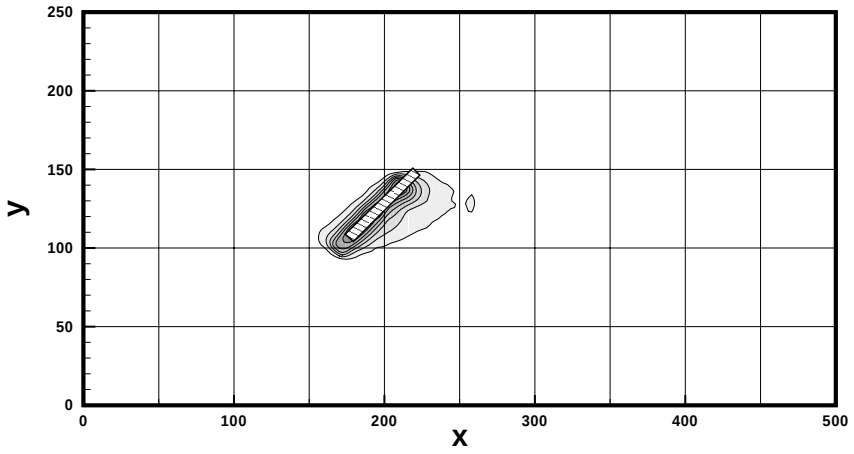

Fig. 10. – Contours of near-ground wind slow-down for the case of obstacle of height 3 meters with respect to the variant with no obstacles.

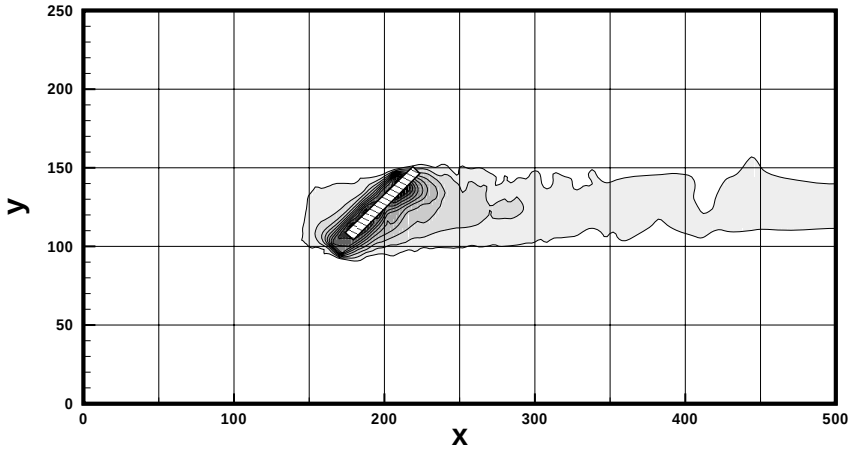

Fig. 11. – Contours of near-ground wind slow-down for the case of obstacle of height 6 meters with respect to the variant with no obstacles.

flow and sediment on the ground. In order to give some hints for evaluation of dust sedimentation, the above mentioned variants of obstacles were evaluated from the point of view of flow speed-up/slow-down at the near-ground level. As the flow slows down, the sedimentation of wind-driven particles becomes more significant and thus to find the regions of decelerated flow is of essential importance. The velocity magnitude fields for all the above-described obstacle configurations were compared with the basic variant without obstacles. This allows us to separate the effect of different obstacles on flow deceleration.

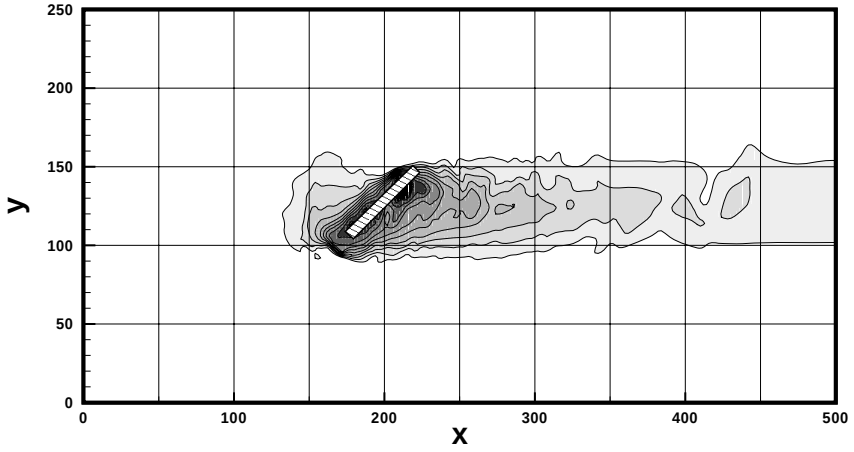

Fig. 12. – Contours of near-ground wind slow-down for the case of obstacle of height 9 meters with respect to the variant with no obstacles.

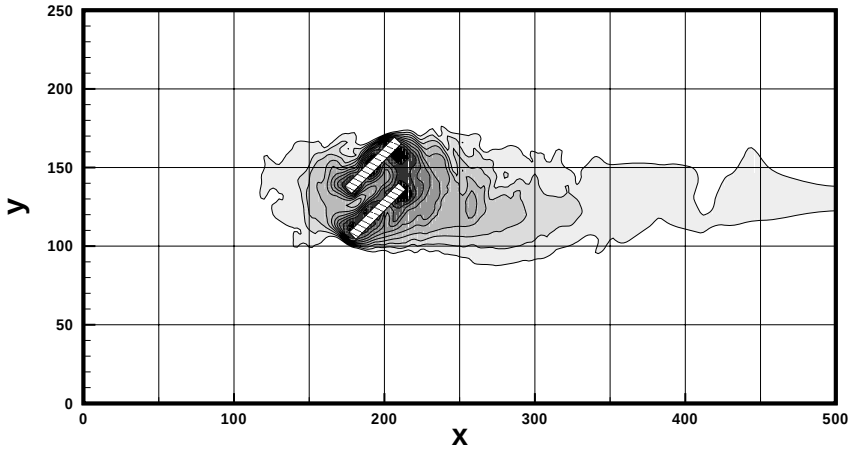

Fig. 13. – Contours of near-ground wind slow-down for the case of two parallel obstacles of height 9 meters with respect to the variant with no obstacles.

Figures 10, 11 and 12 show the case where the obstacle is formed by one single block of height 3, 6 or 9 meters. The contours of the flow deceleration are drawn at the near-ground level where the deposition of wind-drifted particles could occur. The comparison of figs. 10, 11 and 12 again shows the increasing effect of the wind-barriers with their increasing height.

The remaining two variants with two smaller obstacles were compared with the basic case in the same way. The flow deceleration for these cases is drawn in figs. 13 and 14. In order to better understand the effects of different variants of wind-breaking obstacles the detail of both, flow patterns and deceleration contours is drawn for the three most promising variants in figs. 15, 16 and 17. From the comparison of the near-ground wind

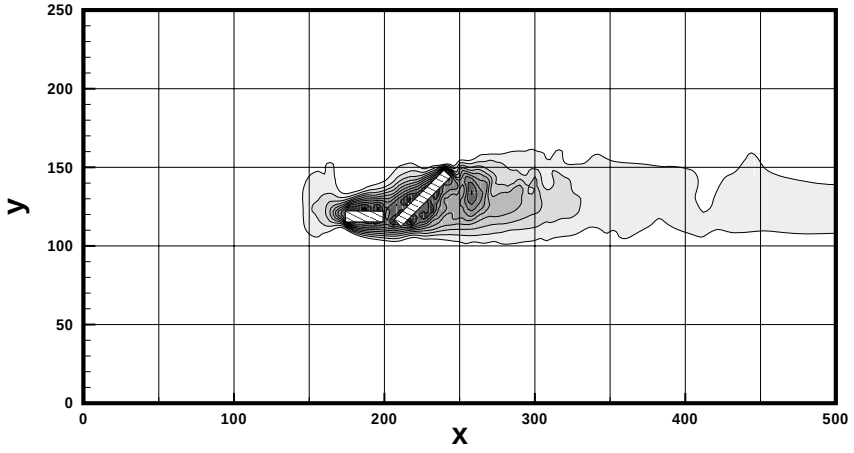

Fig. 14. – Contours of near-ground wind slow-down for the case of two different obstacles of height 9 meters with respect to the variant with no obstacles.

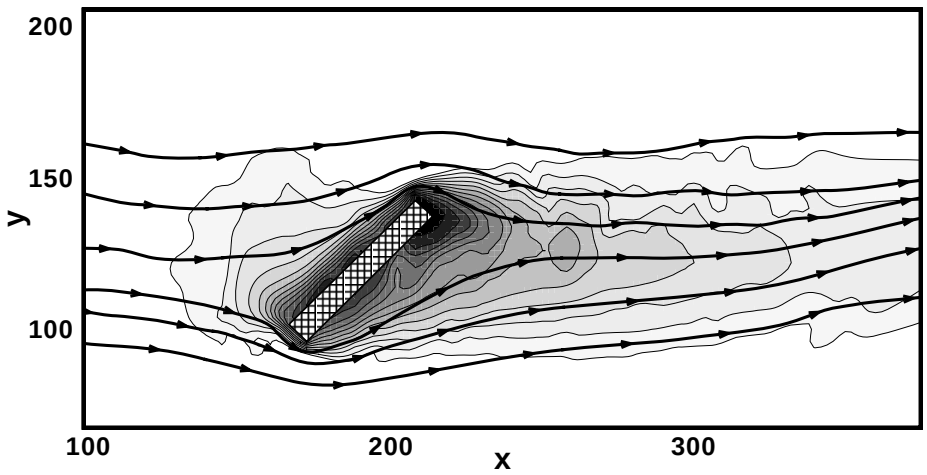

Fig. 15. – Streamlines and contours of wind slow-down at the near-ground level for the case of one large obstacle of height 9 meters with respect to the variant with no obstacles.

slow-down it seems that the variant with two smaller parallel obstacles offers a slightly larger region of flow deceleration and also the local flow deceleration is higher than for the other two variants. Moreover the building area needed for this variant of wind-breakers is a little bit smaller than for the other two cases.

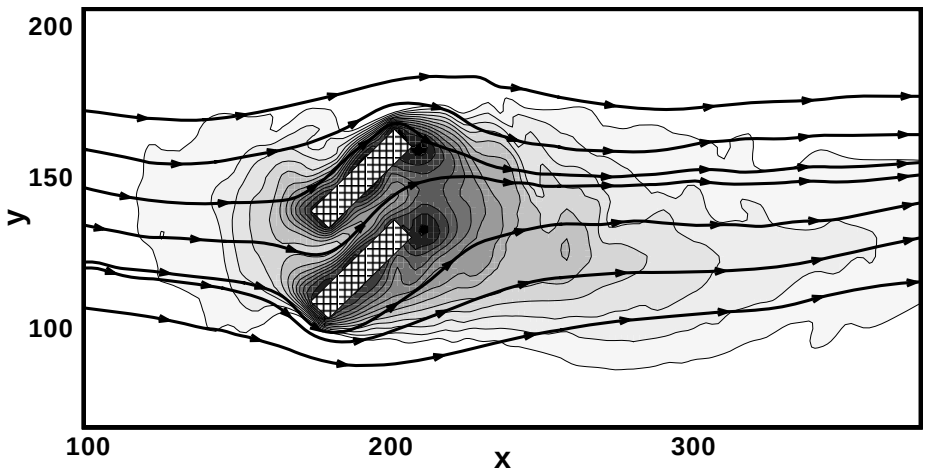

Fig. 16. – Streamlines and contours of wind slow-down at the near-ground level for the case of two parallel obstacles of height 9 meters with respect to the variant with no obstacles.

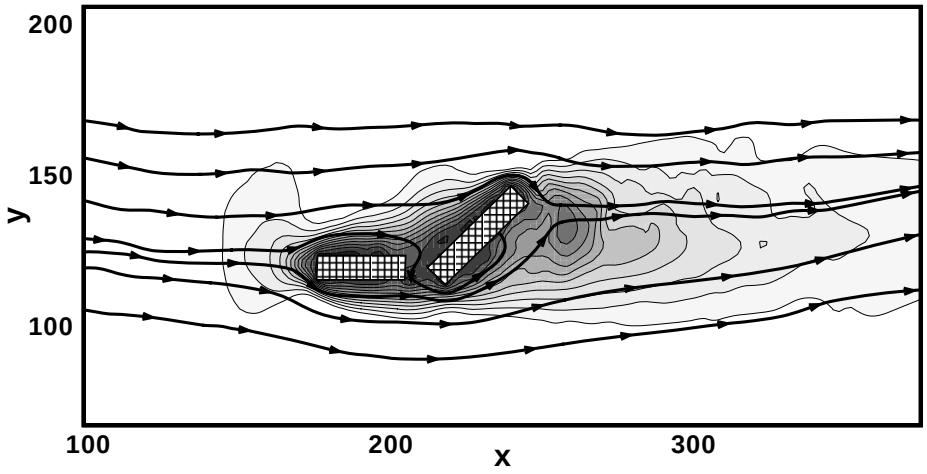

Fig. 17. – Streamlines and contours of wind slow-down at the near-ground level for the case of two different obstacles of height 9 meters with respect to the variant with no obstacles.

4. – Conclusions, remarks

The selected mathematical model is able to properly describe the pollution dispersion problems in complex terrain. Even if more sofisticated models are available for both the flow and the turbulence parametrization, the kind of model used in this study seems to be the right choice for the solution of complex pollution dispersion problems on engineering level.

The numerical method used to solve the set of governing equations has proved sufficient robustness and efficiency for reliable solution of the discussed type of problems. The simple second-order, central in space and time, finite-difference discretization in combination with appropriate artificial viscosity stabilization is very easy to implement and use, so it can be employed without excessive requirements on users and computational resources. The presented numerical simulations have shown that the effect of simulated obstacles has only local impact on the velocity field. This is caused mainly by the complexity of the terrain, where the orography profile involves height changes with scales much larger than the maximum available height of the simulated obstacles. Thus the orography effect is dominant in this case. More detailed study of dust sedimentation should be performed in order to quantify the effects of obstacles on deposition of particles of different sizes. The positive impact of wind-breaking barriers on the deposition of larger particles may be outbalanced by the increase of the turbulent mixing of the smaller particles. Another possible way of the future extension of this study is to assume some of the permeable wind-breaking obstacles, like, *e.g.*, porous fences or forest blocks. This kind of obstacles may be more efficient in dissipating the energy of wind and thus enhancing the sedimentation of airborne particles. The outputs of presented numerical simulations allow very detailed comparison of several variants of wind-barriers. Even simple side-by-side comparison of the above presented figures helps in evaluation of environmental impact and efficiency of the proposed wind-barriers.

* * *

The financial support for the presented project was partly provided by the Grant No. 1ET400760405 and Grant No. 205/06/0727 of the Czech Science Foundation, and by the Research Plan MSM 6840770010 of the Ministry of Education of the Czech Republic.

REFERENCES

[1] Almeida G. P., Durão D. F. G. and Heitor M. V., *Exp. Thermal Fluid Sci.*, **7** (1993) 87.
[2] Ferreira A. D., Silva M. C. G., Viegas D. X. and Lopes A. G., *J. Wind Eng. Ind. Aerodyn.*, **38** (1991) 109.
[3] Ferreira A. D., Lopes A. M. G., Viegas D. X. and Sousa A. C. M., *J. Wind Eng. Ind. Aerodyn.*, **54/55** (1995) 173.
[4] Carpenter P. and Locke N., *J. Wind Eng. Ind. Aerodyn.*, **83** (1999) 109.
[5] Kim H. G., Lee C. M., Lim H. C. and Kyong N. H., *J. Wind Eng. Ind. Aerodyn.*, **66** (1997) 17.
[6] Arya S. P. S. and Shipman M. S., *Atmos. Environ.*, **15** (1981) 1173.
[7] Arya S. P. S., Shipman M. S. and Courtney L. Y., *Atmos. Environ.*, **15** (1981) 1185.
[8] Snyder W. H. and Britter R. E., *Atmos. Environ.*, **21** (1987) 735.
[9] Castro I. P. and Snyder W. H., *Atmos. Environ.*, **16** (1982) 1869.
[10] Gong W. and Ibbetson A., *Boundary-Layer Meteorol.*, **49** (1989) 113.
[11] Gong W., *Boundary-Layer Meteorol.*, **54** (1991) 211.
[12] Crooks G. and Ramsay S., *Boundary-Layer Meteorol.*, **66** (1993) 155.
[13] Arya S. P. S., Capuano M. E. and Fagen L. C., *Atmos. Environ.*, **21** (1987) 753.
[14] Snyder W. H., *Atmos. Environ. A*, **24** (1990) 2071.
[15] Castro I. P. and Apsley D. D., *J. Wind Eng. Ind. Aerodyn.*, **67** & **68** (1997) 375.
[16] Castro I. P. and Apsley D. D., *Atmos. Environ.*, **31** (1997) 839.
[17] Lee S. J. and Kim H. B., *J. Wind Eng. Ind. Aerodyn.*, **80** (1999) 311.
[18] Park C. W. and Lee S. J., *J. Wind Eng. Ind. Aerodyn.*, **91** (2003) 165.
[19] Wang H. and Takle E. S., *Agric. Forest Meteorol.*, **81** (1996) 95.
[20] Wilson J. D. and Yee E., *Agric. Forest Meteorol.*, **115** (2003) 31.
[21] Yaragal S. C., Ram H. S. G. and Murthy K. K., *J. Wind Eng. Ind. Aerodyn.*, **66** (1997) 127.
[22] Packwood A. R., *J. Wind Eng. Ind. Aerodyn.*, **88** (2000) 75.
[23] Lee S. J. and Park C. W., *J. Wind Eng. Ind. Aerodyn.*, **84** (2000) 101.
[24] Lee S. J., Park K. C. and Park C. W., *Atmos. Environ.*, **36** (2002) 1453.
[25] Zaghloul N. A., *Atmos. Model. Software*, **12** (1997) 113.
[26] Park C. W. and Lee S. J., *Atmos. Environ.*, **36** (2002) 2171.
[27] Sládek I., Bodnár T. and Kozel K., *J. Wind Eng. Ind. Aerodyn.*, **95** (2007) 9.
[28] Ould-Dada Z., Copplestone D., Toal M. and Shaw G., *Atmos. Environ.*, **36** (2002) 5595.
[29] Beneš L., Bodnár T., Fraunié Ph. and Kozel K., *Numerical modelling of pollution dispersion in 3D atmospheric boundary layer*, in Sportisse B. (Editor), *Air Pollution Modelling and Simulation* (Springer Verlag) 2002, pp. 69-78.
[30] Bodnár T., Kozel K., Fraunié Ph. and Jaňour Z., *Comput. Visualization Sci.*, **3** (2000) 3.
[31] Bodnár T., Kozel K., Fraunié Ph. and Beneš L., *Numerical modelling of pollution dispersion in complex terrain*, in *Air Pollution IX* (WIT Press) 2001, pp. 85-94.